Available online at www.sciencedirect.com

jmr&t Journal of Materials Research and Technology

www.jmrt.com.br

Original Article

# Processing of $Ti_{50}Nb_{50-x}HA_x$ composites by rapid microwave sintering technique for biomedical applications

*Chander Prakash*[a], *Sunpreet Singh*[b], *Animesh Basak*[c], *Grzegorz Królczyk*[d], *Alokesh Pramanik*[c], *Luciano Lamberti*[e], *Catalin I. Pruncu*[f,g,*]

[a] *School of Mechanical Engineering, Lovely Professional University, Phagwara, Punjab 144411, India*
[b] *Production Engineering, Guru Nanak Dev Engineering College, Ludhiana 141006, India*
[c] *School of Civil and Mech. Eng., Curtin University, GPO Box U1987, Perth, WA 6845, Australia*
[d] *Opole University of Technology, 76 Proszkowska St., 45-758 Opole, Poland*
[e] *Dipartimento di Meccanica, Matematica e Management, Politecnico di Bari, Via Orabona 4, 70126 Bari, Italy*
[f] *Mechanical Engineering, Imperial College London, Exhibition Rd., London SW7 2AZ, UK*
[g] *Mechanical Engineering, School of Engineering, University of Birmingham, Birmingham B15 2TT, UK*

ARTICLE INFO

*Article history:*
Received 5 September 2019
Accepted 21 October 2019
Available online 6 November 2019

*Keywords:*
Orthopaedic implants
Porous $Ti_{50}Nb_{50-x}HA_x$ composite
Rapid microwave sintering
Porosity
Compressive strength
Elastic modulus

ABSTRACT

The main objective of this research is to fabricate porous mechanical-tuned (low elastic modulus and high strength) Ti-based composites with improved bioactivity for orthopaedic applications. Another objective is to demonstrate the potential of microwave sintering and temporary space alloying technique to synthesize porous Ti-based composites. In this study, porous $Ti_{50}Nb_{50-x}HA_x$ ($x = 0$, 10 and 20) composite was fabricated for orthopaedic applications using a powder metallurgical and rapid microwave sintering (PM-RMS) process. Effects of key PM-RMS parameters on the structural porosity, compressive strength, and elastic modulus of built composite were then analysed. The microstructure, pore characteristics, and mechanical properties were investigated in detail. Using high hydroxyapatite (HA) content (20%), short sintering time (5 min), and high compacting pressure (200 MPa) appears to be the best condition among those studied in terms of yielding a high degree of structural porosity (21%) and low elastic modulus (25 GPa) in the sintered composite. Since size of pores in the synthesized composite is in the range of 20–30 μm, structural porosity not only reduces elastic modulus but also enhances bio-activity of sintered composite. The combination of highly porous structure, low elastic modulus, high compressive strength, improved corrosion resistance, and enhanced bioactivity makes porous Ti-Nb-HA composites fabricated by microwave sintering process potential and promising candidates for orthopedic applications.



* *Corresponding author at*: Mechanical Engineering, Imperial College London, Exhibition Rd., London SW7 2AZ, UK.
E-mail: c.pruncu@imperial.ac.uk (C.I. Pruncu).

https://doi.org/10.1016/j.jmrt.2019.10.051

## 1. Introduction

Over the last few decades, titanium-based alloys have extensively been used as biomaterials for orthopaedic implants due to their exceptional biomechanical integrity and excellent bio-activity [1]. However, Ti-based alloys have relatively high elastic modulus (110 GPa) as compared to bone tissues (10–20 GPa). This can lead to stress-shielding that impedes bone remodeling and results in bone resorption and implantation failure [2–4]. To overcome these problems, researchers focused their interest towards the fabrication of porous β-type Ti-alloys [5]. Structural porosity reduces the stiffness of Ti-alloys and results in a reduction of elastic modulus [6,7]. The formation of a β-phase crystalline structure with stabilizing elements (such as Nb and Sn) has also been reported to reduce the elastic modulus of Ti alloys to about 40 GPa [8–15]. This porous structure not only solves the problem of stress shielding but also provides suitable conditions for the tissue growth around the implant [16].

Hydroxyapatite (HA, $Ca_{10}$ $(PO_4)_6(OH)_2$) can be used as an alloying element to promote osseointegration and bioactivity, and to accelerate the bone in-growth support provided by the implant [17–20]. However, there is still a requirement for better designs and manufacturing strategies to produce porous structures rather than the naturally occurring dense ones, transforming the α-Ti to β-Ti microstructure, and tailoring the mechanical integrity to better match the patient's host tissue [5]. A number of β-type Ti-alloys using HA and other stabilizing elements can be fabricated, including Ti-HA [21–23], Ti-Nb [12,13,15,24,25], Ti-Nb-Zr [8,9,15], Ti-Sn-Nb [26,27], Ti-Ni 25,29], Ti-Nb-Zr-x(HA) [30], Ti-Nb-HA [31], and Ti-Nb-Ta-Zr-xHaP [32] alloys. Amongst these materials, HA and Nb-based Ti-alloys gathered much interest from those developing orthopaedic implants, because they possess both low elastic modulus and high HA and Nb content, improving the corrosion resistance of the alloys [21,28,30,31].

Powder metallurgy (PM) is the most widely used method for building porous scaffolds, as it is both cost-effective and allows more control over pore size, pore density, and morphology; it also achieves near-net shape production [33]. PM consists of alloying metallic powders and then sintering the alloyed powder mixture to facilitate the customization of its material composition, mechanical properties, and architectural geometry [34,35].

In earlier decades, various sintering techniques such as convention sintering [36], hot isostatic pressing (HIP) [37], and self-propagating high-temperature synthesis (SHS) [38,39] were utilised. However, these techniques suffer from several disadvantages in terms of high temperature requirements and long sintering times. These parameters influence the uniformity of the microstructure and usually result in coarse grain growth that counters the desired mechanical properties and biomedical performance [40,41]. More recently, microwave sintering (MS) processes produced more uniformly controlled microstructures and porosity in Ti-based alloys [42]. The heating gradient (including heating temperature and heating rate) and time determine microstructure and grain growth [43,44]. Furthermore, since the microwave heating process involves rapid transformation of electromagnetic energy into heat, fine grain growth and a uniform microstructure are easy to be obtained, thus creating a densified, compact material with lower porosity defect rates [45–48]. Microwave sintering is therefore very suited for sintering metallic and ceramic powders in biomedical and other industrial applications [49–52].

Choy et al. [53] synthesized porous Ti-CaP composites using mechanical alloying (MA) and the MS process for biomedical applications. They found that the sintering of the composite including HA formed beta-tricalcium phosphate (β-TCP) and calcium titanate ($CaTiO_3$). Furthermore, they reported that the as-fabricated composites exhibit high porosity and excellent mechanical properties (compressive strength and elastic modulus of 212 MPa and 12 GPa, respectively). These mechanical properties and the bone-like apatite growth of the Ti-CaP composite confirmed its suitability for the orthopaedic industry [54]. Bovand et al. further synthesized Ti-$HA_X$ (X = 10–30%) alloys using MS to study the effect of HA content on structural porosity and hardness of the resulting composite, and higher proportions of HA were found to increase the porosity and hardness of the composite [55].

Biomimetic low-modulus porous Ti-6Al-4V/TiC composite was also developed using the MA and MS process for biomedical applications. The developed composite exhibited a 27% porous structure, 90 MPa compressive strength, 2.9 GPa compressive modulus, and 556 HV micro-hardness. This suggested that the material could potentially be used for load bearing applications [56]. Xu et al. fabricated porous Ni-Ti shape memory composite using the MS technique and studied the effect of pore size on its microstructure, mechanical properties and corrosion resistance [57]. The application of MS for the synthesis of Ti-Nb shape memory composite was also studied, and parametric optimization of the microwave process was carried out to enhance mechanical properties of sintered alloys [58]. Xu et al. further fabricated porous Ti-15MO alloys using PM and MS, achieving 16–50% porosity. However, thery reported that this high degree of structural porosity decreased the mechanical properties of the resulting composite [59].

The available literature does not indicate how to select rapid microwave sintering processes to optimize mechanical properties, geometry and biological performance of $Ti_{50}Nb_{50-x}HA_x$ (x = 0, 10 and 20). In this work, much effort was put in assessing effects of process parameters on structural porosity, compressive strength, elastic modulus and morphological features of the developed composite. In addition, as-prepared samples were characterized in order to assess microscopic changes occurring in material processing.

## 2. Material and methods

Powders of titanium-Ti (99% purity, ≤25 μm), niobium-Nb (99% purity, ≤25 μm), and hydroxyapatite-HA (99% purity, ≤2 μm) were procured from Intelligent Materials Private Limited, India; these were used to synthesise the Ti50Nb50-xHAx composite. Fig. 1 shows the morphology of the raw powders before blending. The powders were mixed to achieve the desired composition of Ti 50%wt, Nb 50-x %wt, and HA x %wt (x = 0, 10, and 20%). The powder mixture was blended in a high emery planetary ball mill (Fritsch, Pulverisette 7) using a tungsten carbide vial and balls, per the processes adopted in pre-

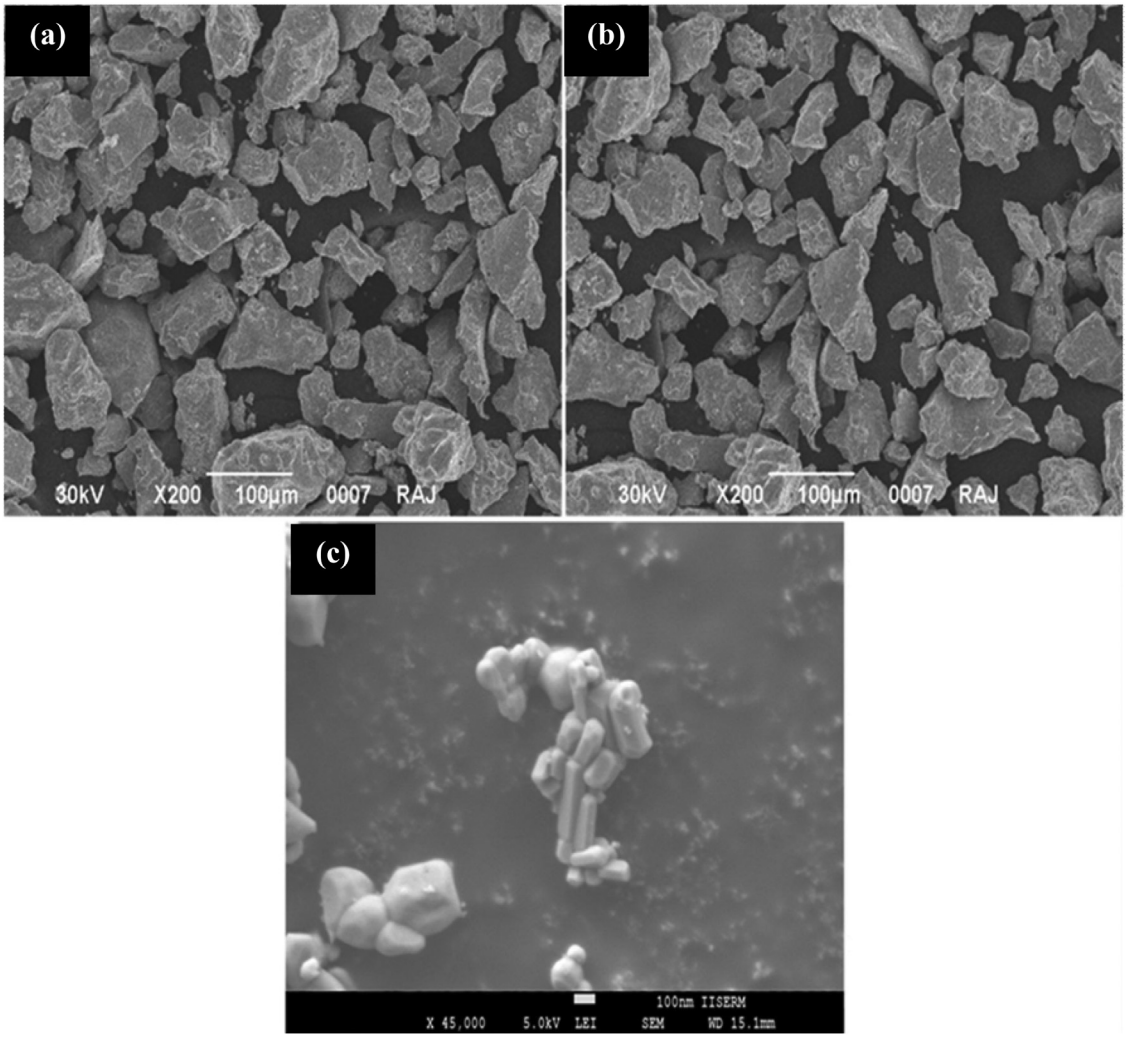


**Fig. 1 – SEM micrographs of raw powders before mechanical alloying (a) Ti, (b) Nb, and (c) HA.**

**Table 1 – Nomenclature of MA-SPS process parameters and corresponding levels considered in this study.**

| Process parameters | Symbol | Units | Levels |
|---|---|---|---|
| HA content | HA | wt.% | 0, 10, 20 |
| Sintering time | $T_s$ | Min | 5, 10, 15 |
| Compacting pressure | $P_c$ | MPa | 100, 150, 200 |

vious research work [60–62]. The powder-to-balls ratio was 1:10. Blending of the composite composition was performed at 200 rpm for about 12 h at ambient conditions. In order to prevent agglomeration and cold welding of the powders, 2% stearic acid was also added to the mixture. After blending, the powder mixture was then compacted into performs of $10 \times 20$ ($\varphi \times L$) mm, at variable pressures, using a mounting. Table 1 presents the nomenclature of the process parameters and the corresponding levels considered in the experiments.

The green compact was then sintered using the rapid microwave sintering process. The experimental set-up for rapid microwave sintering process was developed in-house using a domestic IFB-microwave of 25 L capacity (1400 W, 2.45 HZ). The sintering was carried out for 5 min and the sur-

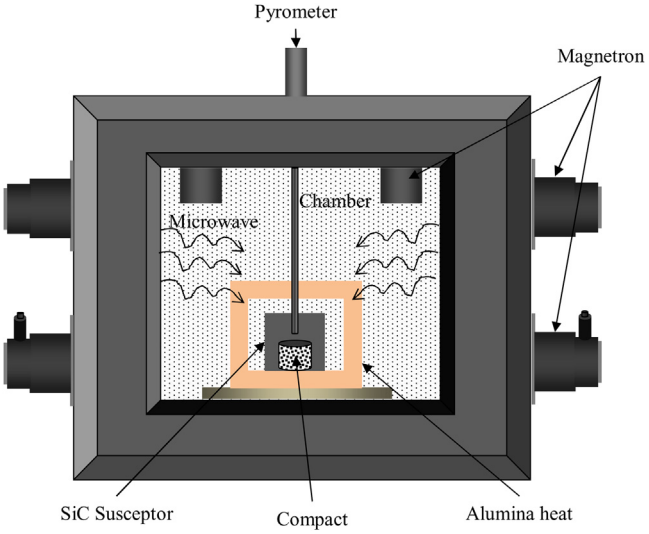


**Fig. 2 – Schematic of the in-house developed experimental setup of rapid microwave sintering process.**

face temperature reached 1500 °C. Fig. 2 presents a schematic diagram of the in-house experimental setup developed for rapid microwave sintering, while Fig. 3 presents the process steps for the synthesis of the $Ti_{50}Nb_{50-x}HA_x$ composite and the sintered dense and porous alloys.

After sintering, microstructure, morphology, elemental and phase composition, structural porosity, and mechanical properties of the sintered $Ti_{50}Nb_{50-x}HA_x$ composite were analysed in detail. Field emission scanning electron microscopy (FE-SEM-7600F by JEOL) and energy dispersive spectroscopy (EDS) were used for the morphological and elemental composition investigations. The working distance for FE-SEM and EDS analysis was 13–15 mm. X-ray diffraction (XRD; X'pert-PRO) was used for evaluating phase composition for the setting of CuKα radiation ~45 kV, current intensity ~40 mA, incident radiation ~2$\theta$. The structural porosity percentage (P) was determined using the formula

$$P = (1 - m/v * \rho) \times 100$$

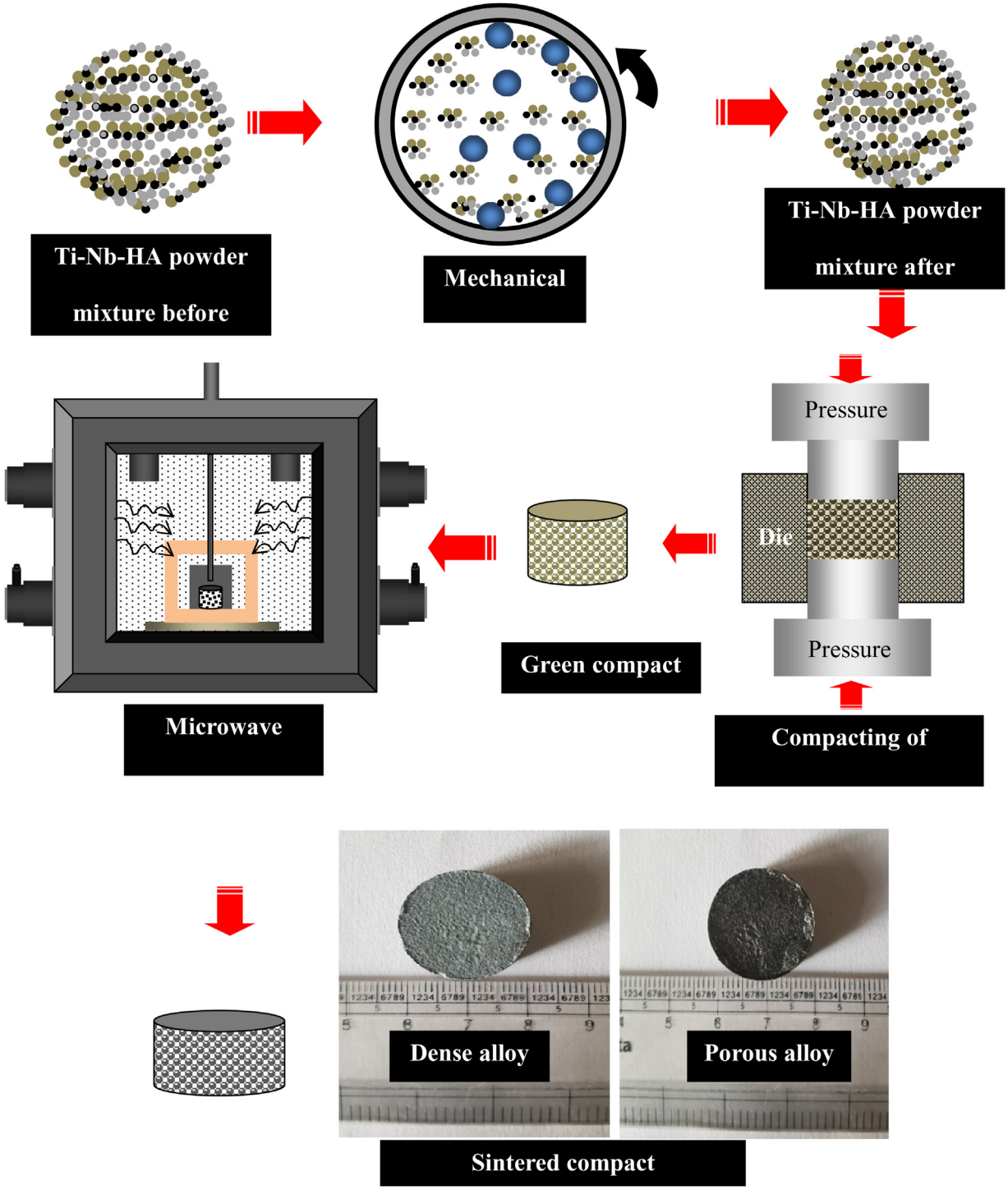


**Fig. 3 – Fabrication route for synthesis of the $Ti_{50}Nb_{50-x}HA_x$ (x = 0, 10, 20) composite and sintered dense and porous alloys.**

**Table 2 – Observed mean and S/N ratio values of porosity, compressive strength, and elastic modulus of the $Ti_{50}Nb_{50-x}HA_x$ sintered composite according to L-9 OA.**

| Sr. no | HA content | Sintering pressure (MPa) | Sintering time (Min) | Porosity | | Compressive strength (MPa) | | Young's modulus (GPa) | |
|---|---|---|---|---|---|---|---|---|---|
| | | | | Mean | S/N ratio | Mean | S/N ratio | Mean | S/N ratio |
| 1 | 0 | 100 | 5 | 13.00 | 21.99 | 751.4 | 57.52 | 50 | −33.98 |
| 2 | 0 | 150 | 10 | 5.00 | 13.89 | 500.3 | 53.98 | 64 | −36.12 |
| 3 | 0 | 200 | 15 | 8.00 | 18.45 | 258.1 | 48.24 | 60 | −35.56 |
| 4 | 10 | 100 | 10 | 12.00 | 21.34 | 823.7 | 58.32 | 54 | −34.65 |
| 5 | 10 | 150 | 15 | 5.00 | 14.50 | 463.8 | 53.33 | 70 | −36.90 |
| 6 | 10 | 200 | 5 | 17.00 | 25.50 | 582.6 | 55.31 | 34 | −30.63 |
| 7 | 20 | 100 | 15 | 14.00 | 22.63 | 391.4 | 51.85 | 50 | −33.98 |
| 8 | 20 | 150 | 5 | 16.00 | 23.95 | 522.3 | 54.36 | 40 | −32.04 |
| 9 | 20 | 200 | 10 | 20.00 | 25.33 | 300.9 | 49.57 | 36 | −31.13 |

where, m, v and ρ are the mass, volume, and theoretical density of the sintered composite, respectively.

Compressive strength and elastic modulus of the sintered composite were determined via compression testing. Cylindrical specimens of dimensions 5 × 10 mm (Diameter × Height) were cut from the sintered alloys. A uniaxial compression test was then conducted at room temperature on the hydraulic UTM testing machine (Model-25, Tinius Olsen) at 0.05 mm/min loading rate. The elastic modulus was calculated based on the initial stage of the stress-strain curve using dedicated software. Deformation was determined from load-displacement curve provided by the testing machine.

## 3. Results and discussion

The results obtained from the RMS process, based on Taguchi's method L-9 OA, are summarized in Table 2. Structural porosity, compressive strength and elastic modulus were measured to quantify the effects of rapid microwave sintering (RMS) process parameters. In Taguchi's method, it is possible to convert output responses into a signal/noise (S/N) ratio serving as output response measurement index. For orthopaedic implant applications, the composite should possess a highly porous structure, low elastic modulus and high compressive strength. Therefore, structural porosity was analyzed in terms of 'higher-the-better', elastic modulus was set as 'lower-the-better', and compressive strength was a 'higher-the-better' type output response characteristic for the development of a $Ti_{50}Nb_{50-x}HA_x$ (x = 0, 10, 20) composite. Using Taguchi's method, the optimal combination of process parameters was determined for the desired level of structural integrity including a highly porous composite structure, good compressive strength, and a low elastic modulus. In the present study, five replicas were performed for each selected combination of parameters.

### 3.1. *Effects of process parameters on sintered material properties*

#### 3.1.1. *Analysis of structural porosity*

Fig. 4 presents the variations of average structural porosity for $Ti_{50}Nb_{50-x}HA_x$ (x = 0, 10, 20) sintered composite with respect to RMS process parameters. It can be seen that average structural porosity tends to increase for higher HA contents.

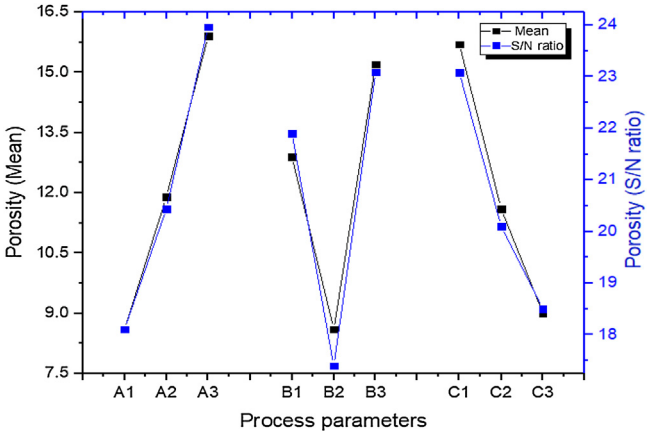


**Fig. 4 – Effect of process parameters on structural porosity. (A1, A2, A3) denote HA content levels; (B1, B2, B3) denote sintering time levels; (C1,C2.C3) denote compacting pressure levels.**

For x = 0 (no HA), densification was extreme and average structural porosity decreased to 8.6%. The lowest structural porosity was 5% at HA = 0%, sintering pressure = 150 MPa, and sintering time = 10 min. The 20% HA content resulted in a much more porous composite ($Ti_{50}Nb_{30}HA_{20}$) with an average structural porosity of 16.66%. The highest structural porosity was 20% at HA = 20%, sintering pressure = 200 MPa, and sintering time = 10 min.

This may be caused by the concourse of two reasons: (i) HA particles are unstable at high temperature and disintegrate during sintering; (ii) HA particles are sacrificed and eroded during grinding and mechanical polishing processes [30]. In general, structural porosity decreased as compacting pressure and sintering time increase. These are the driving forces that remove pores and consolidate the mixture, respectively [31,32]. The average structural porosity hence followed this trend. At high temperature, HA is transformed into β-TCP and CaO, thus increasing porosity. Table 2 shows that average structural porosity of the composite with no HA decreased from 13% to 5% by increasing sintering time from 5 min to 10 min, but then increased to 8% for the very high sintering time. This happened because sintering temperature increases with sintering time, burning the green compact and making

**Table 3 – Results of ANOVA analysis for the parameter combination yielding the highest structural porosity.**

| Source | DF | Seq-SS | Adj-SS | Adj-MS | F | P | % |
|---|---|---|---|---|---|---|---|
| HA | 2 | 99.55 | 99.55 | 49.77 | 112 | 0.009 | 44.53 |
| Pc | 2 | 62.88 | 62.8 | 31.44 | 70.75 | 0.014 | 28.53 |
| Ts | 2 | 60.22 | 60.22 | 30.11 | 67.75 | 0.015 | 26.93 |
| Residual error | 2 | 0.88 | 0.88 | 0.44 | | | 0.004 |
| Total | 8 | 223.55 | | | | | |

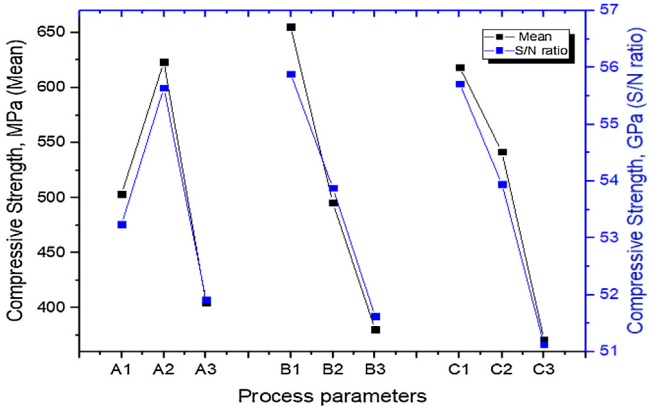


**Fig. 5 – Effect of process parameters on compressive strength. (A1, A2, A3) denote HA content levels; (B1, B2, B3) denote sintering time levels; (C1, C2, C3) denote compacting pressure levels.**

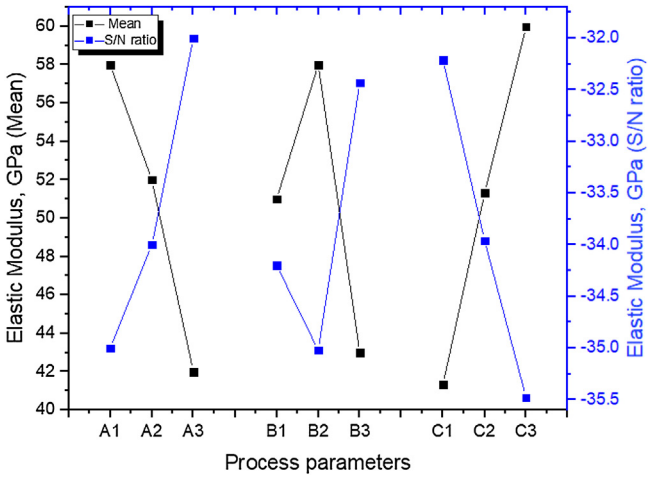


**Fig. 6 – Effect of process parameters on elastic modulus. (A1, A2, A3) denote HA content levels; (B1, B2, B3) denote sintering time levels; (C1, C2, C3) denote compacting pressure levels.**

structure more porous. Average structural porosity decreased from 16% to 9% as compacting pressure passed from 100 MPa to 200 MPa. As per the observed results from the main effect and S/N ratio plots, the third level of HA content (HA = 20%), the third level of sintering pressure ($P_c$ = 200 MPa) and shortest sintering time ($T_s$ = 5 min) yield the highest structural porosity (22.56%) in the $Ti_{50}Nb_{50-x}HA_x$ (x = 0, 10, 20%) sintered composite. Significance level and contribution of each process parameter to the optimal amount of structural porosity were determined using ANOVA. Table 3 shows that HA content is the most significant factor affecting structural porosity (44.53% contribution), followed by compacting pressure (28.53% contribution) and sintering temperature (26.93%). Statistical errors related to unattributed contribution have a marginal effect on variations in porosity (0.004% contribution).

### 3.1.2. *Analysis of compressive strength*

Fig. 5 presents the variation of compressive strength for $Ti_{50}Nb_{50-x}HA_x$ (x = 0, 10, 20%) sintered composite with respect to RMS process parameters. The compressive strength of Ti50Nb50-xHAx (x = 0, 10, 20%) sintered composite became higher by increasing HA content up to 10% but it decreased for the very high HA content. This occurred because HA powder has a small atomic diameter and crystal size, allowing it to easily fill the gaps formed by the Ti and Nb powders, and finally improving mechanical properties of the composite. However, under a combination of higher compacting pressure and longer sintering time, HA changes its crystallographic structure and transforms into β-TCP and CaO, thus forming a porous structure. This limits improvements in mechanical properties.

The maximum compressive strength (876 MPa) of $Ti_{50}Nb_{50-x}HA_x$ sintered composite was achieved for x = 10% HA content, 100 MPa compacting pressure and 5 min sintering time. ANOVA results presented in Table 4 indicate that compacting pressure was the most significant factor affecting compressive strength (40.06% contribution), followed by sintering time (33.74% contribution) and HA content (25.15% contribution). Errors again affect variations in compressive strength just marginally (1.04%).

### 3.1.3. *Analysis of elastic modulus*

Fig. 6 presents the variation of elastic modulus for $Ti_{50}Nb_{50-x}HA_x$ (x = 0, 10, 20%) sintered composite with respect to RMS process parameters. Elastic modulus significantly depends on the structural porosity developed in the sintered composite. Table 2 shows that Young's modulus of the sintered composite decreases with the increase in HA content. This is due to the fact that for higher HA contents, structural porosity increases thus reducing the stiffness of the structure. The elastic modulus decreased overall from 60 GPa to 40 GPa (these values correspond to the average of measured values for HA = 0 and HA = 20%, respectively).

Looking in more detail at the data of Table 2, it can be seen that elastic modulus tends to increase with sintering time although some oscillations in data trend were seen due to the complexity of the process. Since HA particles remain stable at 1050 °C, higher sintering temperature and compaction pressure reduce structural porosity thus increasing density of sintered composite. Longer sintering times make surface

**Table 4 – Results of ANOVA analysis for the parameter combination yielding the highest compressive strength.**

| Source | DF | Seq-SS | Adj-SS | Adj-MS | F | P | % |
|---|---|---|---|---|---|---|---|
| HA | 2 | 71,849 | 71,849 | 35,924 | 24.55 | 0.039 | 25.15 |
| $T_s$ | 2 | 114,427 | 114,427 | 57,214 | 39.1 | 0.025 | 40.06 |
| $P_c$ | 2 | 96,370 | 96,370 | 48,185 | 32.93 | 0.029 | 33.74 |
| Residual error | 2 | 2927 | 2927 | 1463 | | | 1.03 |
| Total | 8 | 285,572 | | | | | |

**Table 5 – Results of ANOVA analysis for the parameter combination yielding the lowest Young's modulus.**

| Source | DF | Seq-SS | Adj-SS | Adj-MS | F | P | % |
|---|---|---|---|---|---|---|---|
| HA | 2 | 99.56 | 99.56 | 49.78 | 34.46 | 0.03 | 31.68 |
| $T_s$ | 2 | 80.89 | 80.89 | 40.44 | 28.00 | 0.03 | 25.74 |
| $P_c$ | 2 | 130.89 | 130.89 | 65.44 | 45.31 | 0.02 | 41.65 |
| Residual error | 2 | 2.89 | 2.89 | 1.44 | | | 0.92 |
| Total | 8 | 314.22 | | | | | |

temperature increase. Hence, HA becomes unstable and disintegrates, thus leading to have a more porous structure with low elastic modulus. Elastic modulus increased for higher compacting pressures. Enhancing compactness of the green compact led to have a highly dense compact sintered composite. Similar behaviour was recently reported in the literature for the Ti-Zr-Nb system [63].

The lowest value of elastic modulus (25 GPa) of sintered material observed in the present experiments was obtained for HA = 20%, Ts = 5 min and Pc = 200 MPa. Table 5 shows the ANOVA results for compressive strength, suggesting that compacting pressure is the most significant factor affecting elastic modulus variation (41.65% contribution), followed by HA content (31.68% contribution) and sintering time (25.74% contribution). Statistical error again makes little contribution (0.92%) to elastic modulus variations.

### 3.2. *Analysis of surface morphology and elemental and phase composition*

As mentioned in the previous sections, optimal settings of process parameters to obtain maximum structural porosity, highest compressive strength, and lowest elastic modulus, correspond to different characteristics of the sintered composite. Table 6 outlines the different types of alloys fabricated using the optimal settings with Taguchi's method. Statistical predictions were confirmed by experimental measurements.

Three types of alloys were fabricated with the various HA percentage contents, as presented in Fig. 7. A highly dense composite ($Ti_{50}Nb_{50}$) was fabricated without adding any HA content.

The possible best conditions for the synthesis of dense $Ti_{50}Nb_{50}$ composite included the first level HA content (HA = 0%), third level sintering time ($T_s$ = 15 min), and second level compacting pressure ($P_c$ = 150 MPa); 2–5% structural porosities were obtained in the synthesized composite. Fig. 7(a–b) shows the morphology and associated EDS spectrum of the resulting $Ti_{50}Nb_{50}$ composite, respectively. The metallographic structure is dense (see Fig. 7(a)) and pore size ranged between 2 and 5 μm. EDS analysis revealed the presence of Ti and Nb elements in the sintered $Ti_{50}Nb_{50}$ composite (see Fig. 7(b)). These results confirmed that no contamination occurred during element alloying or ball milling processes. When HA content was added in the $Ti_{50}Nb_{50-x}HA_x$ (x = 0, 10, 20%) composite porous structure was obtained. The possible best condition for the synthesis of porous $Ti_{50}Nb_{40}HA_{10}$ composite was the second level of HA content (HA = 10%), third level of sintering time ($T_s$ = 15 min), and third level of compacting pressure ($P_c$ = 200 MPa). Fig. 7(c–d) shows the morphology and EDS spectrum of $Ti_{50}Nb_{40}HA_{10}$ composite. It can be clearly seen that the structure was porous and a high degree of structural porosity (18.22%) was observed. The size of pores in the synthesized composite was in the range of 5–10 μm. The EDS spectrum shows the presence on Ti and Nb elements along with Ca, P, and O elements analysis, which confirm that HA disintegrated at high sintering temperature and compacting pressure. Highly porous composite ($Ti_{50}Nb_{30}HA_{20}$) was synthesized when 20% HA content was alloyed. The possible best condition for the synthesis of $Ti_{50}Nb_{30}HA_{20}$ composite was the third level of HA content (HA = 20%), first level of sintering time ($T_s$ = 5 min), and third level of compacting pressure ($P_c$ = 200 MPa). Fig. 7(e–f) shows the morphology and EDS spectrum of $Ti_{50}Nb_{30}HA_{20}$ composite. It can be clearly seen that the structure was porous and a high degree of structural porosity (22.55%) was observed. The size of pores in the synthesized composite was in the range of 20–30 μm. The high intensity of Ca and P in the EDS spectrum confirms the presence of content of HA in the sintered composite.

Fig. 8 shows the XRD pattern of the sintered $Ti_{50}Nb_{50-x}HA_x$ (x = 0, 10, 20) alloys. Peaks of Nb and Ti β-phases can clearly be observed for all alloys. The XRD pattern of sintered $Ti_{50}Nb_{50}$ composite presents α-Ti, β-Ti and Nb phases only. The Nb element is a β-phase stabilizer, assisting the transformation of α-Ti to β-Ti. However, HA is unstable at high-temperature, leading to crystallographic and morphological changes in the structure. The alloying of HA content thus obstacles transformation of α-Ti to β-Ti as HA surrounds the Ti and Nb powder particles, generating a lower diffusion rate between the alloying elements. From the XRD pattern of the $Ti_{50}Nb_{30}HA_{20}$ sintered composite, it can be seen that the intensity of β-phases is lower than those of $Ti_{50}Nb_{40}HA_{10}$ and $Ti_{50}Nb_{50}$ alloys. Moreover, at higher sintering temperatures, the HA disintegrated into Ca, P, and O elements, thus generating various biocompatible phases. $Ca_3(PO_4)_2$, $Ti_5P_3$, and CaO formed dur-

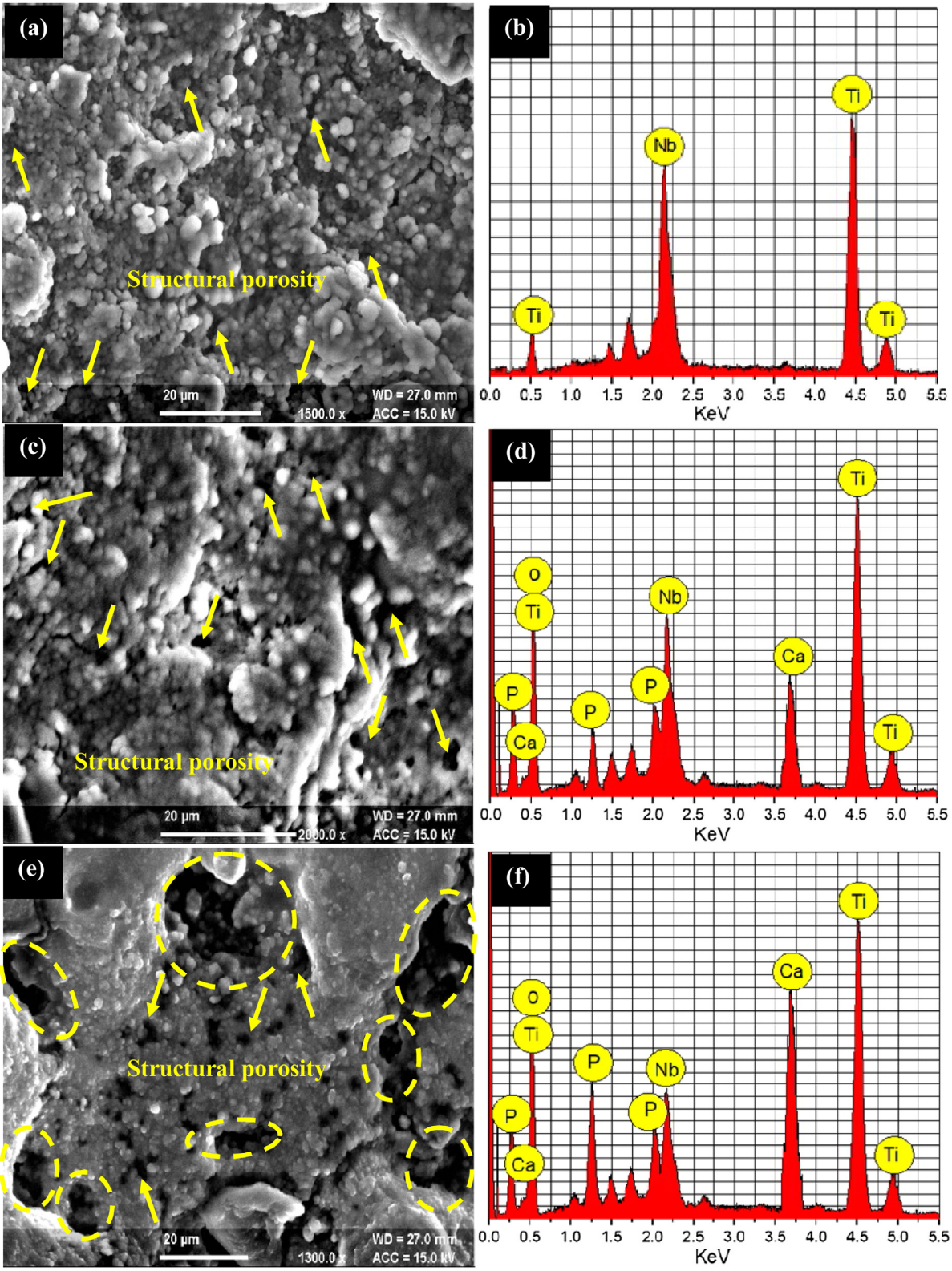


**Fig. 7 – (a) SEM image of the $Ti_{50}Nb_{50}$ composite; (b) EDS spectrum of the $Ti_{50}Nb_{50}$ composite; (c) SEM image of the $Ti_{50}Nb_{40}HA_{10}$ composite; (d) EDS spectrum of the $Ti_{50}Nb_{40}HA_{10}$ composite; (e) SEM image of the $Ti_{50}Nb_{30}HA_{20}$ composite; (f) EDS spectrum of the $Ti_{50}Nb_{30}HA_{20}$ composite.**

**Table 6 – Optimal best conditions for individual output response characteristics with confirmation test.**

| Sr. no | Input process parameters | | | Output response characteristics | | | | | |
|---|---|---|---|---|---|---|---|---|---|
| | HA | $T_s$ | $P_c$ | Predicted | | | Measured | | |
| | | | | Porosity (%) | Compr. strength (MPa) | Young's modulus (GPa) | Porosity (%) | Compr. strength (MPa) | Young's modulus (GPa) |
| 1 | 20 | 5 | 200 | 21 | 383.16 | 24.55 | 19 | 400 | 25 |
| 2 | 10 | 5 | 100 | 15 | 876.63 | 43.55 | 17 | 880 | 46 |
| 3 | 10 | 15 | 150 | 5 | 468.93 | 68.55 | 21 | 475 | 70 |

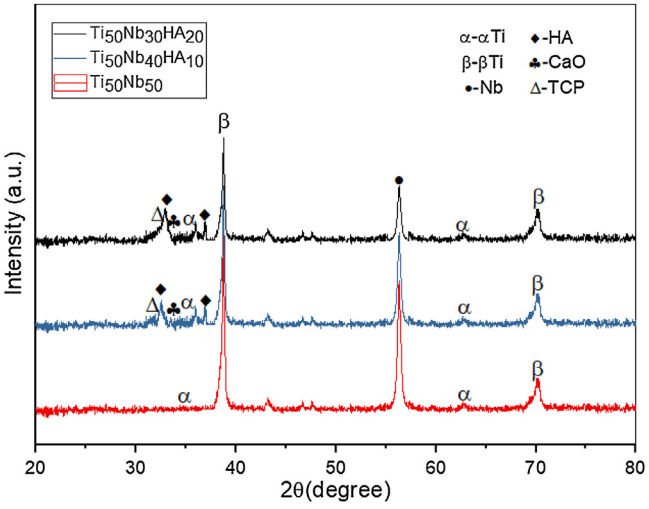


**Fig. 8 – XRD patterns of sintered $Ti_{50}Nb_{50}$, $Ti_{50}Nb_{40}HA_{10}$ and $Ti_{50}Nb_{30}HA_{20}$ alloys.**

ing the sintering of HA with Ti elements is thought to benefit osseointegration performance [19,30–32].

## 4. Conclusions

In this study, porous low elastic and high strength $Ti_{50}Nb_{50-x}HA_x$ (x = 0, 10, 20%) alloys were successfully synthesized using the powder metallurgical process. The study also provided early evidence of the influence of several process variables on the properties of synthesized composite. Higher HA content (20%), short sintering time ($T_s$ = 5 min), and high compacting pressure ($P_c$ = 200 MPa) were found to be the best optimal conditions, where the sintered composite possessed high degree of structural porosity (21%), good compressive strength (383 MPa), and low elastic modulus (25 GPa). The high degree of structural porosity reduced stiffness but degraded mechanical properties of the composite, in particular compressive strength and elastic modulus. HA decomposed at high sintering temperature and compacting pressure, forming various biocompatible phases in the $Ti_{50}Nb_{50-x}HA_x$ composite. Various biocompatible phases such as $Ca_3(PO_4)_2$ (known as TCP), $Ti_5P_3$, and CaO were formed during the sintering process. These are beneficial to the promotion of tissue growth and improve osseointegration between such composite-based implants and natural bone.

In summary, the combination of highly porous structure, low elastic modulus, high compressive strength, improved corrosion resistance, and enhanced bioactivity makes the porous Ti-Nb-HA composites fabricated in this research by microwave sintering process potential and promising candidates for orthopedic applications.

## Conflict of interest

The authors have declared no conflict of interest.

## REFERENCES

[1] Geetha M, Singh AK, Asokamani R, Gogia AK. Ti based biomaterials, the ultimate choice for orthopaedic implants—a review. Prog Mater Sci 2009;54:397–425, http://dx.doi.org/10.1016/j.pmatsci.2008.06.004.

[2] Niinomi M, Nakai M, Hieda J. Development of new metallic alloys for biomedical applications. Acta Biomater 2012;8:3888–903, http://dx.doi.org/10.1016/j.actbio.2012.06.037.

[3] Pradhan S, Singh S, Prakash C, Królczyk G, Pramanik A, Pruncu CI. Investigation of machining characteristics of hard-to-machine Ti-6Al-4V-ELI alloy for biomedical applications. J Mater Res Technol 2019;8:4849–62, http://dx.doi.org/10.1016/j.jmrt.2019.08.033.

[4] Prakash C, Kansal HK, Pabla BS, Puri S, Aggarwal A. Electric discharge machining—a potential choice for surface modification of metallic implants for orthopedic applications: a review. Proc Inst Mech Eng Part B J Eng Manuf 2015;230:331–53, http://dx.doi.org/10.1177/0954405415579113.

[5] Torres-Sanchez C, McLaughlin J, Fotticchia A. Porosity and pore size effect on the properties of sintered Ti35Nb4Sn alloy scaffolds and their suitability for tissue engineering applications. J Alloys Compd 2018;731:189–99, http://dx.doi.org/10.1016/j.jallcom.2017.10.026.

[6] Raza MR, Sulong AB, Muhamad N, Akhtar MN, Rajabi J. Effects of binder system and processing parameters on formability of porous Ti/HA composite through powder injection molding. Mater Des 2015;87:386–92, http://dx.doi.org/10.1016/j.matdes.2015.08.031.

[7] Ryan G, Pandit A, Apatsidis DP. Fabrication methods of porous metals for use in orthopaedic applications. Biomaterials 2006;27:2651–70, http://dx.doi.org/10.1016/j.biomaterials.2005.12.002.

[8] Davidson JA, Mishra A, Kovacs P, Poggie R. New surface-hardened, low-modulus, corrosion-resistant Ti-13Nb-13Zr alloy for total HIP arthroplasty. Biomed Mater Eng 1994;4:231–43.

[9] Bolmaro R, Parau AC, Pruna V, Surmeneva MA, Constantin LR, Avalos, et al. Investigation of cast and annealed Ti25Nb10Zr alloy as material for orthopedic devices. J Mater Res Technol 2019;8:3399–414, http://dx.doi.org/10.1016/j.jmrt.2019.06.006.
[10] Hao YL, Li SJ, Sun SY, Yang R. Effect of Zr and Sn on Young's modulus and superelasticity of Ti–Nb-based alloys. Mater Sci Eng A 2006;441:112–8, http://dx.doi.org/10.1016/j.msea.2006.09.051.
[11] Jung TK, Matsumoto H, Abumiya T, Masahashi N, Kim MS, Hanada S. Mechanical properties-graded Ti alloy implants for orthopedic applications. Mater Sci Forum 2010;631–632:205–10, http://dx.doi.org/10.4028/www.scientific.net/MSF.631-632.205.
[12] Elias CN, Meyers MA, Valiev RZ, Monteiro SN. Ultrafine grained titanium for biomedical applications: an overview of performance. J Mater Res Technol 2013;2:340–50, http://dx.doi.org/10.1016/j.jmrt.2013.07.003.
[13] Li SJ, Cui TC, Hao YL, Yang R. Fatigue properties of a metastable β-type titanium alloy with reversible phase transformation. Acta Biomater 2008;4:305–17, http://dx.doi.org/10.1016/j.actbio.2007.09.009.
[14] García-Garrido C, Gutiérrez-González C, Torrecillas R, Pérez-Pozo L, Salvo C, Chicardi E. Manufacturing optimisation of an original nanostructured (beta + gamma)-TiNbTa material. J Mater Res Technol 2019;8:2573–85, http://dx.doi.org/10.1016/j.jmrt.2019.03.004.
[15] Sun F, Hao YL, Nowak S, Gloriant T, Laheurte P, Prima F. A thermo-mechanical treatment to improve the superelastic performances of biomedical Ti-26Nb and Ti-20Nb-6Zr (at.%) alloys. J Mech Behav Biomed Mater 2011;4:1864–72, http://dx.doi.org/10.1016/j.jmbbm.2011.06.003.
[16] Zhang L, He ZY, Zhang YQ, Jiang YH, Zhou R. Rapidly sintering of interconnected porous Ti-HA biocomposite with high strength and enhanced bioactivity. Mater Sci Eng C 2016;67:104–14, http://dx.doi.org/10.1016/j.msec.2016.05.001.
[17] Prakash C, Singh S, Pabla BS, Uddin MS. Synthesis, characterization, corrosion and bioactivity investigation of nano-HA coating deposited on biodegradable Mg–Zn–Mn alloy. Surf Coat Technol 2018;346:9–18, http://dx.doi.org/10.1016/j.surfcoat.2018.04.035.
[18] Prakash C, Singh S, Singh M, Verma K, Chaudhary B, Singh S. Multi-objective particle swarm optimization of EDM parameters to deposit HA-coating on biodegradable Mg-alloy. Vacuum 2018;158:180–90, http://dx.doi.org/10.1016/j.vacuum.2018.09.050.
[19] Prakash C, Uddin MS. Surface modification of β-phase Ti implant by hydroaxyapatite mixed electric discharge machining to enhance the corrosion resistance and in-vitro bioactivity. Surf Coat Technol 2017;326:134–45, http://dx.doi.org/10.1016/j.surfcoat.2017.07.040.
[20] Yang CY, Lim RM, Wang BC, Lee TM, Chang E, Hang YS, et al. In vitro and in vivo mechanical evaluations of plasma-sprayed hydroxyapatite coatings on titanium implants: the effect of coating characteristics. J Biomed Mater Res 1997;37:335–45, http://dx.doi.org/10.1002/(SICI)1097-4636(19971205)37:3<335::AID-JBM4>3.0.CO;2-M.
[21] Arifin A, Sulong AB, Muhamad N, Syarif J, Ramli MI. Powder injection molding of HA/Ti6Al4V composite using palm stearin as based binder for implant material. Mater Des (1980–2015) 2015;65:1028–34, http://dx.doi.org/10.1016/j.matdes.2014.10.039.
[22] Rastgoo MJ, Razavi M, Salahi E, Mobasherpour I. Spark plasma sintering behavior of hydroxyapatite–titanium nano-composite. J Aust Ceram Soc 2017;53:449–55, http://dx.doi.org/10.1007/s41779-017-0054-6.
[23] Salman S, Gunduz O, Yilmaz S, Ovecoglu ML, Snyder RL, Agathopoulos S, et al. Sintering effect on mechanical properties of composites of natural hydroxyapatites and titanium. Ceram Int 2009;35:2965–71, http://dx.doi.org/10.1016/j.ceramint.2009.04.004.
[24] Dal Bó MR, Salvador CAF, Mello GM, Lima DD, Faria GA, Ramirez AJ, et al. The effect of Zr and Sn additions on the microstructure of Ti–Nb–Fe gum metals with high elastic admissible strain. Mater Des 2018;160:1186–95, http://dx.doi.org/10.1016/j.matdes.2018.10.040.
[25] Lindemann I, Schmidt R, Pilz S, Gebel B, Teresiak A, Gebert A. Ultrafine-grained Ti-40Nb prepared by reactive milling of the elements in hydrogen. J Alloys Compd 2017;729:1244–9, http://dx.doi.org/10.1016/j.jallcom.2017.09.170.
[26] Nouri A, Hodgson PD, Wen CE. Effect of process control agent on the porous structure and mechanical properties of a biomedical Ti–Sn–Nb alloy produced by powder metallurgy. Acta Biomater 2010;6:1630–9, http://dx.doi.org/10.1016/j.actbio.2009.10.005.
[27] Xiong J, Li Y, Wang X, Hodgson P, Wen C. Mechanical properties and bioactive surface modification via alkali-heat treatment of a porous Ti-18Nb-4Sn alloy for biomedical applications. Acta Biomater 2008;4:1963–8, http://dx.doi.org/10.1016/j.actbio.2008.04.022.
[28] Köhl M, Habijan T, Bram M, Buchkremer HP, Stover D, Koller M. Powder metallurgical near-net-shape fabrication of porous NiTi shape memory alloys for use as long-term implants by the combination of the metal injection molding process with the space-holder technique. Adv Eng Mater 2009;11:959–68, http://dx.doi.org/10.1002/adem.200900168.
[29] Li DS, Zhang YP, Ma X, Zhang XP. Space-holder engineered porous NiTi shape memory alloys with improved pore characteristics and mechanical properties. J Alloys Compd 2009;474:L1–5, http://dx.doi.org/10.1016/j.jallcom.2008.06.043.
[30] He YH, Zhang YQ, Jiang YH, Zhou R. Effect of HA (hydroxyapatite) content on the microstructure, mechanical and corrosion properties of (Ti13Nb13Zr)-xHA biocomposites synthesized by sparkle plasma sintering. Vacuum 2016;131:176–80, http://dx.doi.org/10.1016/j.vacuum.2016.06.015.
[31] Bhushan B, Singh A, Sing R, Mehta JS, Gupta A, Prakash C. Fabrication and characterization of a new range of β-type Ti-Nb-Ta-Zr-xHaP (x = 0, 10) alloy by mechanical alloying and spark plasma sintering for biomedical applications. Mater Today Proc 2018;5:27749–56, http://dx.doi.org/10.1016/j.matpr.2018.10.010.
[32] Singh R, Singh B, Gupta A, Prakash C. Fabrication and characterization of Ti–Nb–HA alloy by mechanical alloying and spark plasma sintering for hard tissue replacements. IOP Conf Ser: Mater Sci Eng 2017;225.
[33] Sharma N, Kumar K. Mechanical characteristics and bioactivity of porous Ni50-xTi50Cux (x = 0, 5 and 10) prepared by P/M. Mater Sci Technol 2018;34:934–44, http://dx.doi.org/10.1080/02670836.2017.1412041.
[34] Sharma B, Vajpai SK, Ameyama K. Microstructure and properties of beta Ti–Nb alloy prepared by powder metallurgy route using titanium hydride powder. J Alloys Compd 2016;656:978–86, http://dx.doi.org/10.1016/j.jallcom.2015.10.053.
[35] Xiong JY, Li YC, Wang XJ, Hodgson PD, Wen CE. Titanium–nickel shape memory alloy foams for bone tissue engineering. J Mech Behav Biomed Mater 2008;1:269–73, http://dx.doi.org/10.1016/j.jmbbm.2007.09.003.
[36] Zhu SL, Yang XJ, Hu F, Deng SH, Cui ZD. Processing of porous TiNi shape memory alloy from elemental powders by Ar-sintering. Mater Lett 2004;58:2369–73, http://dx.doi.org/10.1016/j.matlet.2004.02.017.

[37] Yuan B, Chung JP, Zhang X, Zeng MQ, Zhu M. Control of porosity and superelasticity of porous NiTi shape memory alloys prepared by hot isostatic pressing. Smart Mater Struct 2005;14, http://dx.doi.org/10.1088/0964-1726/14/5/005.
[38] Tosun G, Ozler L, Kaya M, Orhan N. A study on microstructure and porosity of NiTi alloy implants produced by SHS. J Alloys Compd 2009;487:605–11, http://dx.doi.org/10.1016/j.jallcom.2009.08.023.
[39] Zhao Y, Taya M, Kang Y, Kawasaki A. Compression behavior of porous NiTi shape memory alloy. Acta Mater 2005;53:337–43, http://dx.doi.org/10.1016/j.actamat.2004.09.029.
[40] Singh S, Gupta D, Jain V, Sharma AK. Microwave processing of materials and applications in manufacturing industries: a review. Mater Manuf Process 2015;30:1–29, http://dx.doi.org/10.1080/10426914.2014.952028.
[41] Loharkar PK, Ingle A, Jhavar S. Parametric review of microwave-based materials processing and its applications. J Mater Res Technol 2019;8:3306–26, http://dx.doi.org/10.1016/j.jmrt.2019.04.004.
[42] Tang CY, Wong CT, Zhang LN, Choy MT, Chow TW, Chan KC, et al. In situ formation of Ti alloy/TiC porous composites by rapid microwave sintering of Ti6Al4V/MWCNTs powder. J Alloys Compd 2013;557:67–72, http://dx.doi.org/10.1016/j.jallcom.2012.12.147.
[43] Mondal A, Upadhyaya A, Agrawal D. Microwave sintering of W-18Cu and W-7Ni-3Cu alloys. J Microw Power Electromagn Energy 2009;43:11–6, http://dx.doi.org/10.1080/08327823.2008.11688598.
[44] Padmavathi C, Upadhyaya A, Agrawal D. Effect of sintering temperature and heating mode on consolidation of Al-7Zn-2·5Mg-1Cu aluminum alloy. Bull Mater Sci 2012;35:823–32, http://dx.doi.org/10.1007/s12034-012-0369-4.
[45] Agrawal DK. Microwave processing of ceramics. Curr Opin Solid State Mater Sci 1998;3:480–5, http://dx.doi.org/10.1016/S1359-0286(98)80011-9.
[46] Mondal A, Agrawal D, Upadhyaya A. Microwave sintering of refractory metals/alloys: W, Mo, Re, W–Cu, W–Ni–Cu and W–Ni–Fe alloys. J Microw Power Electromagn Energy 2010;44:28–44, http://dx.doi.org/10.1080/08327823.2010.11689768.
[47] Oghbaei M, Mirzaee O. Microwave versus conventional sintering: a review of fundamentals, advantages and applications. J Alloys Compd 2010;494:175–89, http://dx.doi.org/10.1016/j.jallcom.2010.01.068.
[48] Plucknett KP, Wilkinson DS. Microstructural characterization of a microwave-sintered silicon nitride based ceramic. J Mater Res 1995;10:1387–96, http://dx.doi.org/10.1557/JMR.1995.1387.
[49] Choy MT, Tang CY. Effect of porosity on compressive yield strength of microwave sintered titanium components. Key Eng Mater 2015;626:97–102, http://dx.doi.org/10.4028/www.scientific.net/KEM.626.97.
[50] Han J-K, Song H-Y, Saito F, Lee B-T. Synthesis of high purity nano-sized hydroxyapatite powder by microwave-hydrothermal method. Mater Chem Phys 2006;99:235–9, http://dx.doi.org/10.1016/j.matchemphys.2005.10.017.
[51] Sha L, Liu Y, Zhang Q, Hu M, Jiang Y. Microwave-assisted co-precipitation synthesis of high purity β-tricalcium phosphate crystalline powders. Mater Chem Phys 2011;129:1138–41, http://dx.doi.org/10.1016/j.matchemphys.2011.05.075.
[52] Tang CY, Zhang LN, Wong CT, Chan KC, Yue TM. Fabrication and characteristics of porous NiTi shape memory alloy synthesized by microwave sintering. Mater Sci Eng A 2011;528:6006–11, http://dx.doi.org/10.1016/j.msea.2011.04.040.
[53] Choy M-T, Tang C-Y, Chen L, Law W-C, Tsui C-P, Lu WW. Microwave assisted-in situ synthesis of porous titanium/calcium phosphate composites and their in vitro apatite-forming capability. Compos Part B Eng 2015;83:50–7, http://dx.doi.org/10.1016/j.compositesb.2015.08.046.
[54] Bovand D, Yousefpour M, Rasouli S, Bagherifard S, Bovand N, Tamayol A. Characterization of Ti-HA composite fabricated by mechanical alloying. Materi Des (1980–2015) 2015;65:447–53, http://dx.doi.org/10.1016/j.matdes.2014.09.021.
[55] Xu J, Zhang J, Bao L, Lai T, Luo J, Zheng Y. Preparation and bioactive surface modification of the microwave sintered porous Ti-15Mo alloys for biomedical application. Sci China Mater 2018;61:545–56, http://dx.doi.org/10.1007/s40843-017-9098-2.
[56] Choy MT, Tang CY, Chen L, Wong CT, Tsui CP. In vitro and in vivo performance of bioactive Ti6Al4V/TiC/HA implants fabricated by a rapid microwave sintering technique. Mater Sci Eng C 2014;42:746–56, http://dx.doi.org/10.1016/j.msec.2014.06.015.
[57] Xu JL, Bao LZ, Liu AH, Jin XF, Luo JM, Zhong ZC, et al. Effect of pore sizes on the microstructure and properties of the biomedical porous NiTi alloys prepared by microwave sintering. J Alloys Compd 2015;645:137–42, http://dx.doi.org/10.1016/j.jallcom.2015.05.006.
[58] Ibrahim MK, Hamzah E, Saud SN, Nazim EM, Bahador A. Parameter optimization of microwave sintering porous Ti-23%Nb shape memory alloys for biomedical applications. Trans Nonferrous Met Soc China 2018;28:700–10, http://dx.doi.org/10.1016/S1003-6326(18)64702-8.
[59] Xu LJ, Xiao SL, Tian J, Chen Y-Y. Microstructure, mechanical properties and dry wear resistance of β-type Ti-15Mo-xNb alloys for biomedical applications. Trans Nonferrous Met Soc China 2013;23:692–8, http://dx.doi.org/10.1016/S1003-6326(13)62518-2.
[60] Prakash C, Singh S, Gupta MK, Krolczyk G, Khanna N. Synthesis, characterization, corrosion resistance and in-vitro bioactivity behavior of biodegradable Mg–Zn–Mn–(Si–HA) composite for orthopaedic applications. Materials 2018;11, http://dx.doi.org/10.3390/ma11091602.
[61] Prakash C, Singh S, Pabla BS, Sidhu SS, Uddin MS. Bio-inspired low elastic biodegradable Mg–Zn–Mn–Si–HA alloy fabricated by spark plasma sintering. Mater Manuf Process 2019;34:357–68, http://dx.doi.org/10.1080/10426914.2018.1512117.
[62] Prakash C, Singh S, Verma K, Sidhu SS, Singh S. Synthesis and characterization of Mg–Zn–Mn–HA composite by spark plasma sintering process for orthopedic applications. Vacuum 2018;155:578–84, http://dx.doi.org/10.1016/j.vacuum.2018.06.063.
[63] Yan XH, Jang M, Yong Z. High-throughput screening for biomedical applications in a Ti–Zr–Nb alloy system through masking co-sputtering. Sci China Ser G Phys Mech Astron 2019;62, http://dx.doi.org/10.1007/s11433-019-9387-7. Paper No. 996111.